
Near Infrared Camera
and
Multi-Object Spectrometer
READY FOR LAUNCH
UNIVERSITY OF ARIZONA
BALL
GSFC
NICMOS
THE SECOND GENERATION
HUBBLE SPACE TELESCOPE
G. Schneider, R. Thompson,
M. Rieke, E. Mentzell (U. of Az.)

ABSTRACT

The Near Infrared Camera and Multi-Object Spectrometer (NICMOS) is a second-generation instrument to be installed on the Hubble Space Telescope (HST) during the February 11, 1997 on-orbit servicing mission. Integration, testing, and ground-calibration of NICMOS were completed in September, 1996. Expected instrumental performance figures were ascertained in two extensive system level thermal vacuum calibration tests employing external radiometric flat-field, spectral/wavelength, and polarization stimuli. Optical performance was verified and quantified using the Refractive Abberated Simulator/Hubble Opto-Mechanical Simulator at Ball Aerospace. On-orbit operations and electro-mechanical interfaces were tested and verified in a series of activities carried out in the HST Vehicle Electrical and Systems Test facility at the Goddard Space Flight Center. The results of these calibrations and tests have been transferred to the Space Telescope Science Institute for general use in planning and analyzing NICMOS observations, and on-orbit check-out and calibration. We report here on major aspects of those elements of NICMOS instrumental and system performance, as determined from these tests and calibrations, which should be understood by potential users of the instrument. Support for this work was provided by NASA through contract number NAS5-31289.

LAUNCH READINESS UPDATE

The University of Arizona formally transferred ownership of NICMOS to the U.S. Government (NASA) on December 19, 1996 following a successful final pre-shipment review. NICMOS was shipped from Ball Aerospace Technologies Corp. (BATC) in Boulder, Colorado to Hanger AE at the Kennedy Space Flight Center (KSC) on December 27, 1996. NICMOS is now in the shuttle Vertical Processing Facility and will soon be moved to Pad 39-A. A final recool of the N_2 cryogen to 50K will take place on the pad soon thereafter.

INSTRUMENT OVERVIEW

- **3 Cameras with Close, Spatially Non-Contiguous Fields-of-View**
- **Spectral Sensitivity:** **$0.8\mu m \leq l \leq 2.5\ \mu m$**
- **Detectors:** **256^2 Photodiode Arrays (HgCdTe on Sapphire) Si MUX, 4 Quads; Non-destructive R/Os**
- **Operating Temps.:** **FPAs at 58K, Spectral Elements at 155K**
- **Spectral Elements:** **48 Filters, 6 Polarizers, 3 Grisms, 3 Blanks**
- **Field Offset Mechanism for Non-intrusive Background Measures**

CAMERA	1	2	3
FIELD OF VIEW	11"	19.2"	51.2"
PIXEL SCALE	43 mas	75 mas	200 mas
DIFFR. LIMIT	to 1.0 μm	to 1.75 μm	
UNIQUE ATTRIBUTES	"Short" λ's (≤ 1.9 μm)	Coronograph (0.3" Radius)	Grism Spectra (r ~200)

NICMOS will provide infrared imaging and spectroscopic observations of astronomical targets in the spectral range 0.8-2.5 µm. NICMOS is an HST Axial Replacement Instrument, containing three cameras designed for simultaneous operation*. NICMOS will replace the Faint Object Spectrograph.

The NICMOS optics present the detectors with three adjacent, but not spatially contiguous Fields-of-View of different image scales. NICMOS employs three low noise, high Quantum Efficiency, HgCdTe 256×256 Focal Plane Arrays (FPAs) in a passive dewar using solid N_2 as a coolant. Thermoelectric cooling will prolong the nominal mission lifetime to approximately 4.3 years. Each camera carries a complement of 20 spectral elements, selected through three independent Filter Wheel Mechanisms. Grism spectroscopy, in the widest field camera (number 3) provides a multi-object spectrographic capability with a resolution of 200. A 0.3 arc-second radius occulting spot and optimized cold mask in the intermediate resolution camera (number 2) provides a coronographic imaging capability. Polarimetric imaging may be carried out in cameras 1 or 2.

The NICMOS Fore-Optics Assembly fully corrects the spherically aberrated HST input beam. NICMOS will achieve diffraction limited performance in the high resolution camera (number 1) to 1.0 µm, and in camera 2 to 1.75 µm. An internal Field-Offset Mechanism allows NICMOS to observe background fields and in parallel with other HST instruments without re-pointing the spacecraft.

* Parfocal operation of Camera 3 with Cameras 1/2 is not anticipated until the dewar fully relaxes after some cryogen loss.

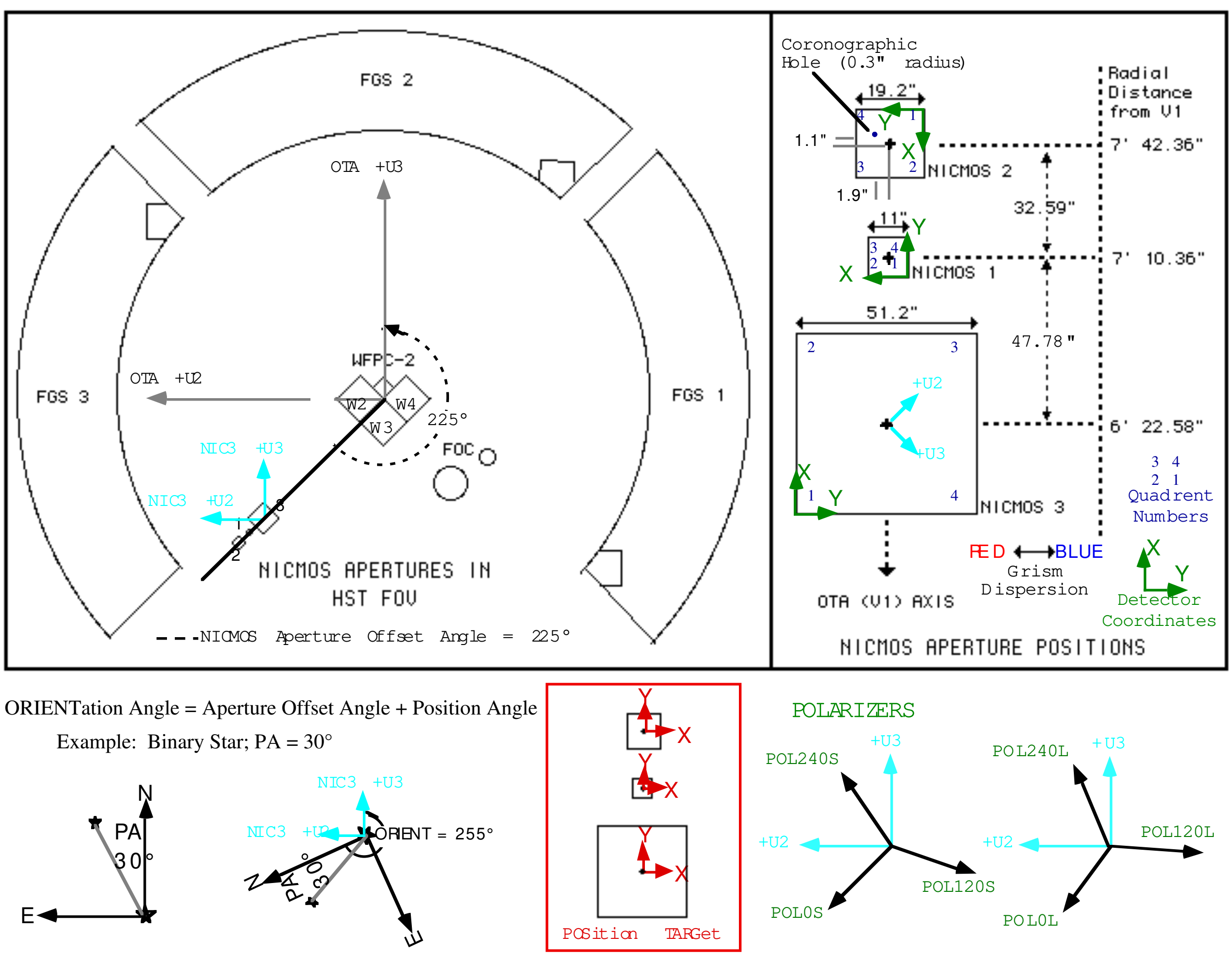

Aperture locations for nominal parfocal setting of the Pupil Alignment Mirror.

OPTICAL ALIGNMENT & VERIFICATION

The integrated NICMOS optical system is comprised of both "cold" and "warm" elements. The cold components, namely the filters, grisms, and polarizers on three filter wheels, the cold pupil masks, and the focal plane arrays, are installed in the dewar. The warm components (fifteen mirrors) are mounted to a graphite epoxy truss called the Fore-Optics Bracket (FOB). The FOB also supports the mechanisms for the Field-Offset Mirror (FOM) which provides aberration correction, field offset, and flat field illumination. All of the mirrors were put into their nominal positions, by adjusting them in six degrees of freedom, within a coordinate and angle measurement facility called the FOB Alignment System (FAS). Fine adjustments to the FOB, using the FAS, were made to reach the performance goals for image quality and HST pupil imaging. Full cavity double-pass interferometric tests were possible here, thanks to an aberrated reference sphere, which generates the spherical aberration present in the HST wavefront. Results indicate that the anamorphic asphere on the surface of the FOM is nicely correcting the HST optical aberrations.

After FOB alignment and environmental testing optical performance was verified in a second HST simulator. The Refractive Aberration Simulator and the Hubble Opto-Mechanical Simulator (together RAS/HOMS) was used to verify the performance of COSTAR. Along with the HST spherical aberration, it provides the full field aberrations of the HST (astigmatism and field curvature), and generates the proper HST exit pupil. RAS/HOMS was originally set up to simulate HST at only one wavelength (0.6328 microns). It has been enhanced for NICMOS use by the addition of an 0.81 micron diode laser source, which is just visible at the short end of the HgCdTe detectors' bandpass. Prior to complete integration the NICMOS FOB relayed simulated images from RAS/HOMS to a Photometrics CCD camera placed where the three detector are now located. This provided a very accurate and sensitive picture of the imaging performance and permitted the verification of the performance of the field offset mirror and its mechanisms.

Following the integration of the FOB and dewar into the main NICMOS truss the Pupil Adjust Mirror (PAM) and its mechanisms were installed along with source delivery systems for an internal Flat Field Illuminator (FFI). The integrated instrument was returned to RAS/HOMS for system level testing. Adjustment of the PAM to get the system focused and HST pupil image centered on the corrector mirror prior to shipping NICMOS to GSFC for acoustic vibration testing was done here. The alignment processes allowed for zero-gravity release compensation expected on-orbit.

SYSTEM LEVEL THERMAL VACUUM TEST & CALIBRATION

NICMOS underwent an extensive series of thermal balance, engineering checkout, and instrument calibration tests in the 20 foot "Brutus" thermal vacuum chamber at BATC during the summer of 1996 to fully validate, quantify, and calibrate numerous aspects of the instrument performance. In three separate runs, NICMOS was operated by both real-time and stored command sequences using the SITS ground system - a full analog to the HST command and control system. A total of 126,370 image frames and ~8 Gb of engineering data (more than 28.9 Gb in all) were obtained in carrying out 82 separate planned and derived calibration activities and engineering tests. Nearly all planned goals of the SLTV program were met, a few derivative calibration activities will be carried into the on-orbit Servicing Mission Observatory Verification (SMOV) program. Reduced calibration data sets and reference files have been delivered to the Space Telescope Science Institute (STScI) for use in the OPUS pipeline.

HST INTEGRATION, COMPATIBILITY AND OPERATIONS TESTS

In October, NICMOS underwent a series of integration and operations tests at GSFC's Vehicle Electrical Simulation and Test (VEST) facility. VEST is a high-fidelity replica of the HST electrical and mechanical systems. Mechanical fit checks, electrical interface and systems compatibility tests (power systems, command and data handling, etc.) and crew familiarization activities were carried out here. While in the VEST, NICMOS was operated by the Space Telescope Operations Control Center in a series of on-orbit servicing and science mission simulations.

GRISM WAVELENGTH CALIBRATION

Camera 3 carries a set of three grisms which, combined, span the usable wavelength range of the NICMOS detectors. The central wavelengths of the grisms are evenly spaced, logarithmically, to provide a constant spectral resolution of ~200. This resolution represents a compromise between spectral and spatial range, limiting flux, optical alignment sensitivity, and wedge angle subject to the physical constraints of the filter wheel. Bandpass isolation is achieved by the application of interference filter coatings on the front faces of the Grisms.

GRISM DESIGN CRITERIA

GRISM	CENTRAL λ	BANDPASS	WEDGE ANGLE	LINES/mm
G096	0.9639	0.8 – 1.2	5.5219°	45.00
G141	1.4099	1.1 – 1.9	5.5889°	30.77
G206	2.0583	1.4 – 2.5	5.6944°	21.05

The NICMOS grisms were tested and calibrated using an external optical stimulus and wavelength calibrator. The "GRism Abberated VALidator" (GRAVAL) presented a single field point in NICMOS camera 3 with optical aberrations identical to the HST. The imaging and optical components of GRAVAL were placed in the Brutus thermal vacuum chamber with NICMOS. Krypton line and quartz halogen continuum lamps, residing in a source delivery system outside of the chamber , were coupled to GRAVAL by a fiber feed through the chamber wall.

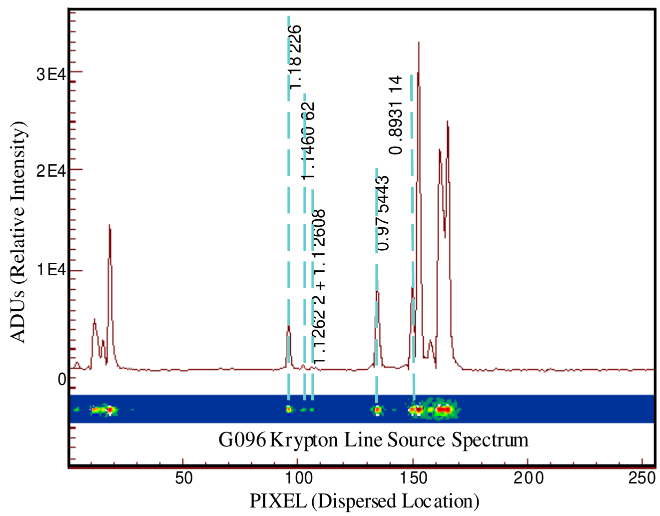

Absolute wavelength calibrations for each of the three grisms, for both first and second order spectra were obtained. The effect of the grisms on the width of the PSF was also examined.

GRISM WAVELENGTH AND SPATIAL CALIBRATIONS

GRISM	PIXEL SCALE (Å/pixel)		R		TILT[1]	OFFSET[2]
	1st Order	2nd Order	1st Order	2nd Order		(Pixels)
G096	53.9	27.3	178.8	353.1	3.2°	4.63
G141	77.8	~40.1	181.2	351.6	0.8°	7.05
G206	110.5	58.1	186.3	354.3	1.7°	2.13

1) The direction of spectral dispersion is tilted slightly with respect to the Y-axis of the detector arrays.
2) Grism spectra are spatially displaced, by small numbers of pixels, relative to an undispersed (filter) image.

BROADENING[3] OF PSF BY GRISMS

GRISM	PSF FWHM (Pixels)		FILTER	PSF FWHM (Pixels)	
	1st Order	2nd Order		@1st Order	@2nd Order
G096	2.14	1.78	F110W	1.38	1.26
G141	2.14	1.93	F175W	1.41	1.42
G206	2.38	2.28	F204W	1.42	1.38

3) While our figure of merit is the FWHM, broadening of the PSF due to the grisms is predominanly in the low-amplitude wings of the PSF.

The NICMOS spectral elements are cooled by the flow sublimated N_2 vapor. Because of the long cooling times these calibrations were performed with the grisms warmer than the expected ~150K on-orbit equilibrium temperature. Since the line ruling spacings will vary with temperature recalibration during SMOV will be carried out.

FLAT FIELD CALIBRATION

Flat field calibrations were obtained using both an internal flat field illuminator (FFI), and an external NIST traceable external absolute radiometric calibration unit. The latter "Calibrated InfraRed sourCE" (CIRCE) was located in the thermal vacuum chamber in close physical proximity to NICMOS and presented an overfilled uniform illumination source to the NICMOS entrance aperture. Cross-calibration to the FFI was performed since an external absolute calibrator will not be available on orbit. Flat field maps (i.e., responsivity calibrations for each pixel in the arrays) for all filter/camera combinations were obtained with S/N > 300.

REPRESENTATIVE FLAT FIELDS*

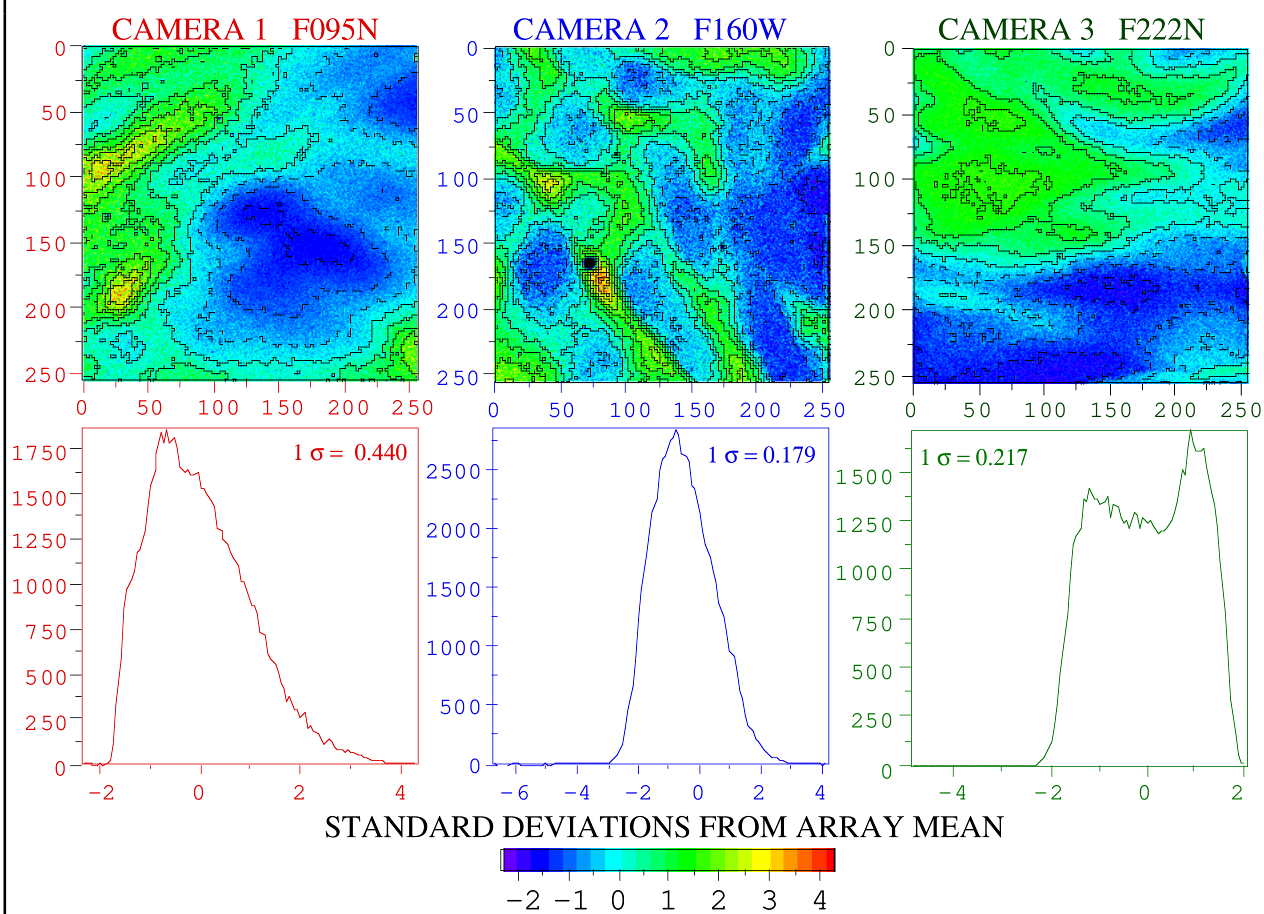

*Images have been smoothed with a 3x3 box-car to better illustrate the structure of large spatial scale variations

The NICMOS arrays exhibit both pixel-to-pixel and large spatial scale variations in response which are highly wavelength dependent. The morphology of the flat fields at all wavelengths correlates extremely well with the detector gain maps and hence little structure is introduced by the NICMOS optics. The variations in response over all spatial scales is greatest at short wavelength, becoming very flat near the long wavelength cutoff of the devices. The dispersions widths of the pixel response functions are similar in Cameras 1 and 3. The QE variations in Camera 2 are about half the amplitude of those seen in Cameras 1 and 3. Knowing the structure of the flat-field response one may judiciously place targets in intrinsically flat, or, high QE regions of the fields of view.

READOUT NOISE

The readout noise characteristics of the three flight detectors for each of the readout modes were ascertained. In general, this systemic noise component is approximately 30e⁻ with a distribution function across all pixels with a FWHM of about 8 electrons for a single final minus single initial readout of an array. The non-destructive readout capability of the NICMOS arrays, however, is exploited by the detector operations and imaging S/W where the read noise can be reduced by reading out a FPA multiple times. A variety of sampling strategies were tested during SLTV in different operating regimes in an effort to both optimize standard sets of readout patterns and understand the trade-offs between reducing read noise while increasing amplifier (corner) glow. The modes which benefit from this are Accumulate (MIF) and Multiple Accumulate (MultiAccum).

Accumulate mode produces the difference of the average of N reads at the start of the integration (initial) and N reads at the end of the integration (final). The differencing and averaging is done by the on-board S/W and only a single image is returned to the ground. Readouts may be spaced by either 0.203s (in "Fast" mode), or 2.837s (in "slow" mode). In MultiAccum mode a series of arbitrarily spaced readouts (quantized at 13ms) are stored and downlinked to the ground.

ACCUMULATE MODE

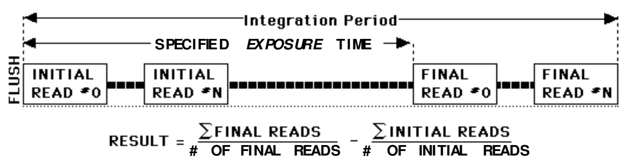

MULTIACCUM MODE

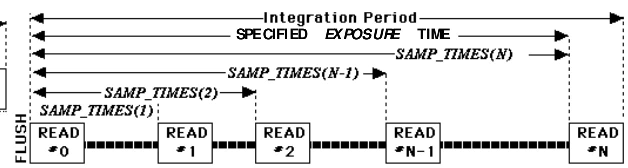

ACCUMULATE MODE READ NOISE (electrons)

INTEGRATION TIME:	132s/FAST			525s/FAST			2090s/FAST			132s/SLOW		
# of I/F READS:	1	9	25	1	9	25	1	9	25	1	9	25
CAMERA 1	38	13	15	36	15	16	33	14	15	19	23	36
CAMERA 2	28	12	13	30	13	14	23	12	13	23	20	23
CAMERA 3	31	14	15	31	16	16	28	16	16	36	32	37

MULTIACCUM MODE READ NOISE (electrons) with 26 READOUTS

INTEGRATION TIME:	PATTERN 1	PATTERN 2	PATTERN 3
CAMERA 1	23	16	17
CAMERA 2	22	20	19
CAMERA 3	25	17	19

```
Pattern 1 = 525s,  evenly spaced reads
Pattern 2 = 525s,  9 I/F reads @ 0.203s spacing, rest evenly distributed
Pattern 3 = 2090s, spacing: powers of 2 to 256s, then linear 128s
```

While the 4 quadrants of each FPA has it own set of readout electronics, the readout noise characteristics of all quads in an FPA are very similar. The accompanying figure demonstrates this for quadrants 1 and 4 of Camera 1. Similar behavior is seen amongst all quadrants for each of the arrays with the integrated flight readout electronics.

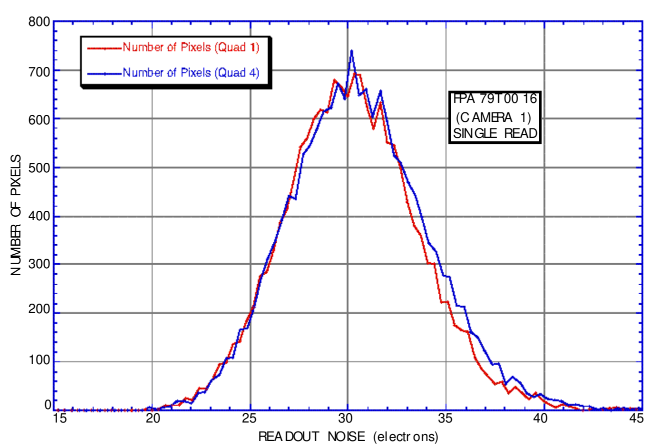

AMPLIFIER GLOW

The NICMOS FPAs possess on-chip amplifiers located near the corners of each separately read-out quadrant. When enabled, the amplifiers emit a low-level "glow" which elevates the background in the array corners. During the ~203ms required to read through an entire array (for all modes except Bright Object mode) approximately 300e- are deposited in the pixels closest to the corners of the array for each non-destructive readout. The repeatability of this phenomena was confirmed during SLTV demonstrating the ability to calibrate this effect out of raw image frames. The increase in the DC level of perimeter pixels, however, effectively decreases the dynamic range and results in a spatially variant S/N for a spatially uniform input. Thus, the S/N achievable in the center of the array is better, for a given multiple-read sequence, than at the corners.

This composite of nine 2090-second dark frames taken in SLTV illustrates a number of features which may be seen in raw NICMOS image frames.

1) Enhanced background in the corners is due to amplifier glow.
2) Twenty-pixel wide horizontal banding artifacts are induced by reclocking after resetting to reduce shading.
3) The "dark lines" and vertical gradient in the reclocked regions are due to shading.
4) The appearance of quadrant boundaries is due to small differences in DC offsets between the quadrants.
5) The peppering of the frame by particle hits due to cosmic rays (CRs). The CR event rate on-orbit is expected to be approximately an order of magnitude higher than in our test chamber. Hence, the coaddition of these nine frames produces a CR hit rate which would be typical of a near orbit-long image.

All but the last (5) may be removed in calibration by the appropriate application of reference frames such as those obtained in SLTV. The NICMOS IDT has developed algorithms for rejection and compensation of CR hits from single MultiAccum data sets or multiple Accum data sets.

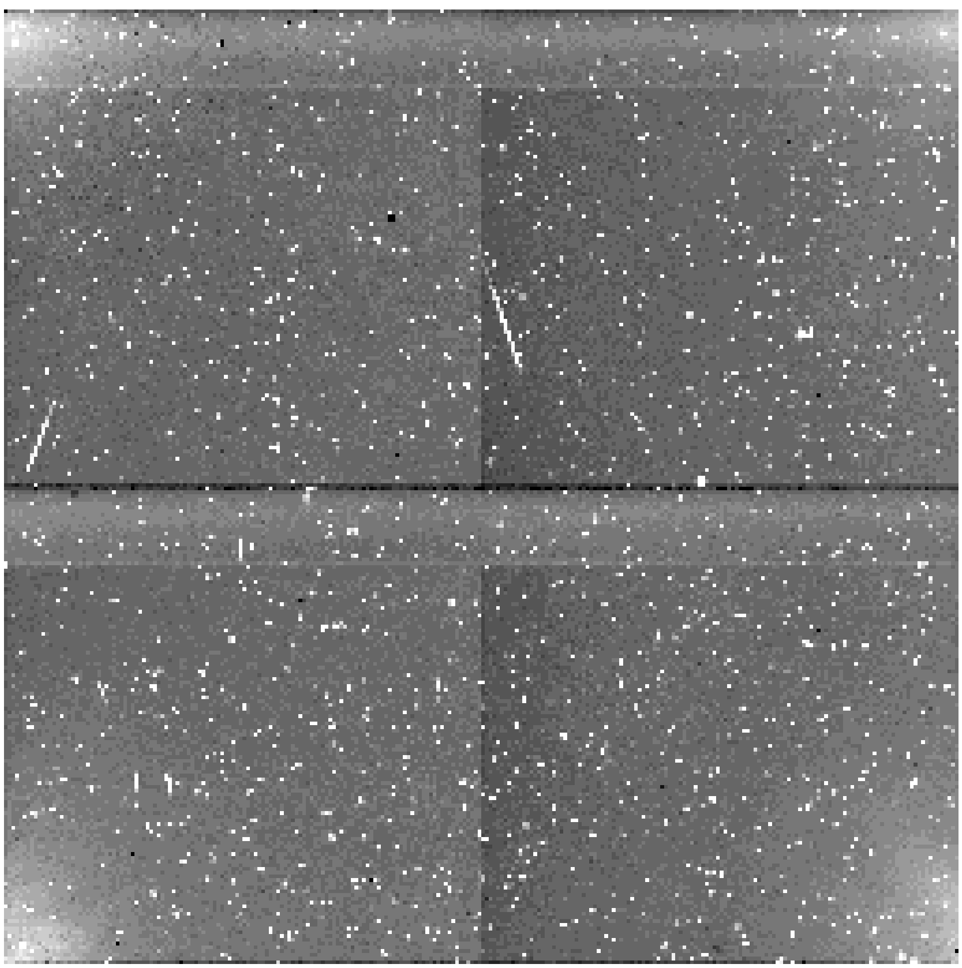

DETECTOR GAINS

The NICMOS read out electronics employ 16-bit Analog-to-Digital converters, providing an effective dynamic range of approximately 12 stellar magnitudes in a single readout. Each pixel in each of the three flight detectors has a specific conversion gain , i.e., the number of deposited electrons required to produce a single measured count, or "data number" out of the converters. A direct determination of the conversion gains was made using CIRCE as a stimulus during SLTV. and gain maps for all three detectors have been assembled.

There is significant pixel-to-pixel variation in the conversion gains for a given detector and the gain maps must be employed to ascertain the actual net charge in a given pixel. In general the aggregate behavior over all pixels in each of the three arrays may be characterized as illustrated below:

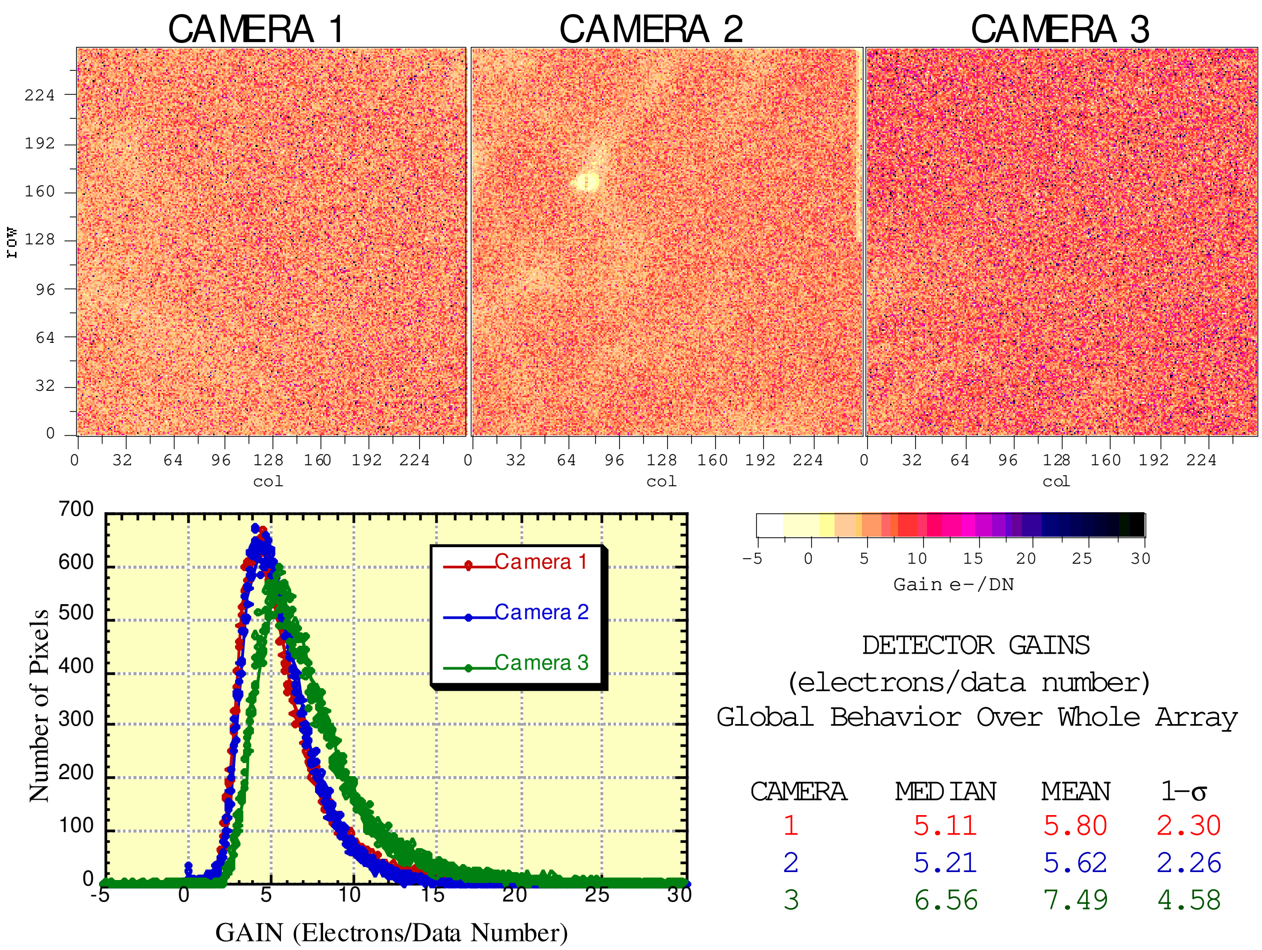

DETECTOR GAINS
(electrons/data number)
Global Behavior Over Whole Array

CAMERA	MEDIAN	MEAN	1-σ
1	5.11	5.80	2.30
2	5.21	5.62	2.26
3	6.56	7.49	4.58

Both the pixel-to-pixel variations in gain and the larger scale features seen in the gain maps are imprinted in the wavelength-dependent flat fields. These may be removed in calibration using reference files which have been prepared from SLTV data and delivered to STScI.

LINEARITY and SATURATION

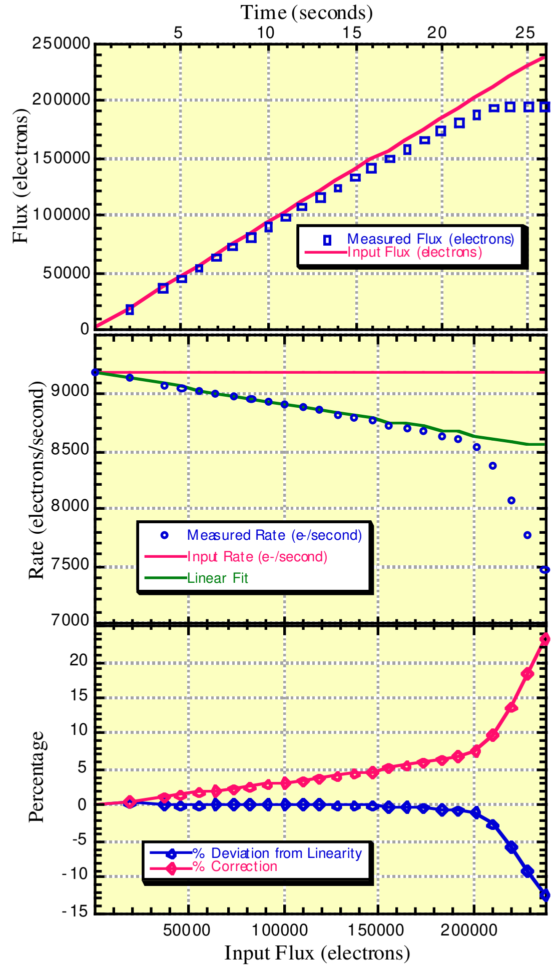

The NICMOS FPAs exhibit essentially linear response over most of their useful dynamic range. The measured rate of charge deposition for a given photodiode declines, linearly, until the charge approaches that pixel's well capacity. When a pixel is fully saturated continuing exposure to incident flux produces no increase in measured signal level, and indeed may actually exhibit a slight decline. This behavior is such that one can identify three regimes of operation:

1) The lower ~80% of the dynamic range where residuals resulting from a simple linear correction are less then a few tenths of a percent.

2) A region beyond this but before saturation turn-over where the data require a non-linear correction.

3) The saturation region where data are uncorrectable and unrecoverable.

Both the linear and non-linear portions of the response curves are highly repeatable and have been characterized on a pixel-by-pixel basis for each of the three detectors. Calibration reference files which define nodal points delineating these regions, as well as coefficients for first and second order corrections have been developed and provided to STScI. Linearity corrections, based upon this characterization, will be performed in the data reduction pipeline for the non-saturated regions of detector performance.

The accompanying figure illustrates the regimes of linear, non-linear, and saturated behavior for a representative pixel in Camera 1 whose conversion gain is that of the array median.

DARK CURRENT

The NICMOS FPAs have intrinsically very low dark currents and better their original requirements by a factor of more than 20. Dark currents for each pixel in the three detectors were measured during SLTV after the optical blanks located in the vapor cooled shield were sufficiently cold so as not to significantly contribute a thermal background which could be construed as a contributor to the dark currents. Dark currents were measured with the detectors biased at slightly smaller voltages than will be used on-orbit (430mv as opposed to 500mv), and hence the dark currents may be slightly different. Recognizing this, dark currents will be remeasured and calibrated during SMOV. None-the-less, the change in dark current (if any) will be a small fraction of the SLTV measured dark currents, which may be characterized as follows over all pixels in each detector:

MEDIAN DARK CURRENTS (electrons/second)

CAMERA 1	CAMERA 2	CAMERA 3
0.153 ± 0.02	0.146 ± 0.02	0.237 ± 0.02

- Derived from MultiAccum Pattern 3 (see READOUT NOISE)
- Corner amplifier glow increases overall median values

SHADING

The NICMOS FPAs exhibit a noiseless signal gradient orthogonal to the direction of primary clocking (horizontal in flight) referred to as "shading". The magnitude of the shading signal is dependent upon:

- Time between a pixel read and the last reset in it's row.
- Pixel Clock Rate (the "readout duration").
- FPA Column Number (similar functional forms, but different scaling).

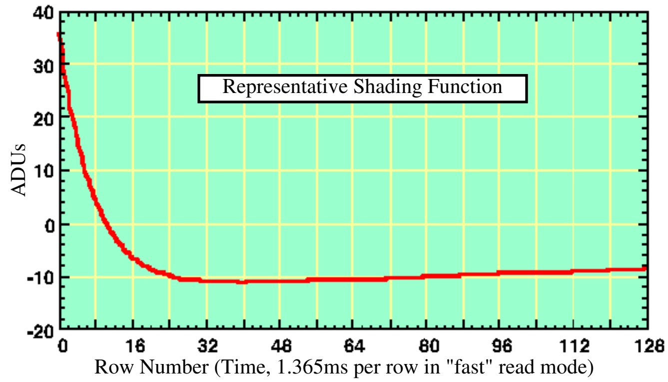

The shading gradient may be represented, approximately, by a non-linear function of the form:

$$\text{ADUs} = c1 + [\, c2 \times \ln(1 + \text{time})^{0.5}\,] + c3 \times \text{time}$$

where: c1 is related to kTC noise & DC offset
c2 is a measure of the shading amplitude (for each column)
c3 is a measure of the dark current (for each pixel)

However, shading is absolutely repeatable for image frames clocked and read out in exactly the same manner (with a given set of electronics). In data calibration the subtraction of dark frames of identical inter-read integration times and clock rate will remove the shading signature. For this reason the NICMOS IDT recommended to STScI the adoption of standard integration sample sequences (for MultiAccum mode) and stepped integration times (for Accum mode) for shading calibration purposes. These sequences and times have been incorporated into the NICMOS flight S/W and now constitute the standard methods of using these modes by STScI.

In an effort to reduce the magnitude of the shading signature in uncalibrated image frames, a sequential double addressing scheme is employed for the pixels in the first 20 rows in the array. Following the final (of 3) global reset cycles which precede each integration, an initial read of the array begins immediately. The first 20 rows of pixels are non-destructively read (at a 10.5 µsec rate for "fast mode"). The address pointer is reset to pixel zero of each quadrant, and the sequential read through the array without interruption. This process does significantly reduce (but not eliminate) the shading gradient, but in itself introduces a low-level artifact. The rows of pixels which have been reclocked have slightly elevated DC levels, which appear as broad horizontal bands. These, however, are absolutely repeatable and are removed in the subtraction of identically clocked dark frames.

The shading functions for all three flight arrays were calibrated during SLTV. As a result of contemporaneous SLTV testing, however, the nominal commanded detector bias voltages (which will be used on-orbit) were raised by 70 millivolts which invalidated this calibration. Recalibration in SLTV was not possible due to schedule constraints and new shading corrections will be obtained in SMOV and during HST Cycle 7.

PERSISTENCE

When the NICMOS arrays are not integrating they are placed in an "auto-flush" mode which is designed to continually remove residual charge from each pixel. Data from a variety of SLTV tests suggested the existence of an image persistence-like phenomena in all three cameras indicating that this process may not have been working as anticipated based upon experience with ground-based NICMOS arrays. The observed image latency and decay did not have quite the behavior associated with understood potential causes of image persistence. In an attempt to both better understand and possibly provide a remedy for this phenomenon a revised auto-flush pattern was developed and tested on the instrument in late December following it's return to BATC from GSFC. As a result of this testing we now have more insight as to the nature of the problem, but the attempted "fix" (which pre-dated this testing itself) did not elevate the problem.

The accompanying figure illustrates the problem from the post-SLTV persistence testing. Following exposure to light, a detector was read-out multiple times with non-destructive MultiAccum sequences. The figure shows the temporal decrement in measured charge accumulation rate as a function of time before background correction. The three curves are for 11x11 pixel areas of Camera 1 which have intrinsically High, Medium, and Low sensitivity under the banddpass of the filter used. In background corrected data the time required for the residual image to decay to is quite long. It had been conjectured that the additional pixel accesses themselves would help alleviate the apparent image persistence. To investigate this, following the pre-readout exposure to light, sequences of very short (.6s) single read-pair Accum dark exposures were taken with 0, 3, and 10 contiguous repetitions before the MultiAccum readouts.

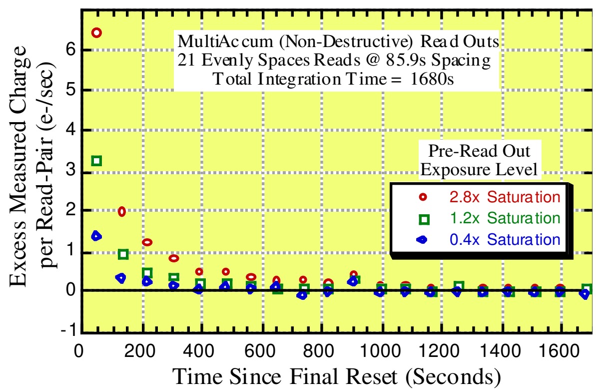

The residual persistence measured by the MultiAccum frames was invariant with the insertion of "extra" appropriately timed readouts. This implied that the persistence is strictly a function of time since the prior illumination. Similar, lower amplitude behavior, can be seen in pre-exposure background data with a decay time constant which is very similar to the post-illuminated data themselves. This suggests that some effect other than persistence in the detector array may be the cause of what is seen. This could be due to a stabilization effect in the output amplifiers, which are only enabled during readouts in the flight system. This conjecture requires further investigation. Disabling of the amplifiers except during reads reduce the parasitic heat leak into the dewar.

Quantitatively, after subtracting the backgrounds, the degree of this persistance-like phenomenon was seen to be less than the read-noise for exposures which were pre-illuminated to ~ 40% of full-well depth for the first read following illumination, and declined exponentially thereafter. The 1/e folding time for this decay was ~23 seconds for Camera 1.

PERSISTENCE ON FIRST READ AFTER ILLUMINATION

QE of Region	Saturation Level	Persistance (e-/sec).*
"Low"	40%	<0.1
"Medium"	120%	2.5
"High"	280%	5.3

*Background Corrected

Observers are urged to take note of this phenomenon and should consider how this may effect the design and interpretation of their observations.

SUSCEPTIBILITY TO COSMIC RAYS

The potential degradation of performance of the NICMOS arrays due to radiation damage was previously ascertained by subjecting a non-flight FPA to accelerated accumulation at the Harvard cyclotron. No device failure (MUX latch-up, dead pixels, etc.) was seen even when the FPA was subjected to 10 times expected lifetime dosage. Following exposure to severe dosage elevated levels of dark currents were seen which decayed over several minutes. Operationally, this may be the determining factor in setting the trailing edge of our SAA avoidance contour. Over the expected lifetime of the instrument small elevations in the dark currents may be expected.

As a byproduct of other testing in SLTV we serendipitously were able to ascertain the effects of cosmic ray hits on NICMOS image data. The cosmic ray event rate, on orbit, is expected to be approximately an order of magnitude higher than on the ground. By stacking many long dark calibration frames pulse-height distributions and event rate estimates were obtained. From these we expect NICMOS images, on orbit, to be effected by CR events at a rate of about 0.6 pixels per second. We note that this is comparable to WFPC-2 when one compensates for the difference in geometrical sizes of NICMOS pixels (40x40 microns) as compared to WFPC-2 pixels (15x15 microns).

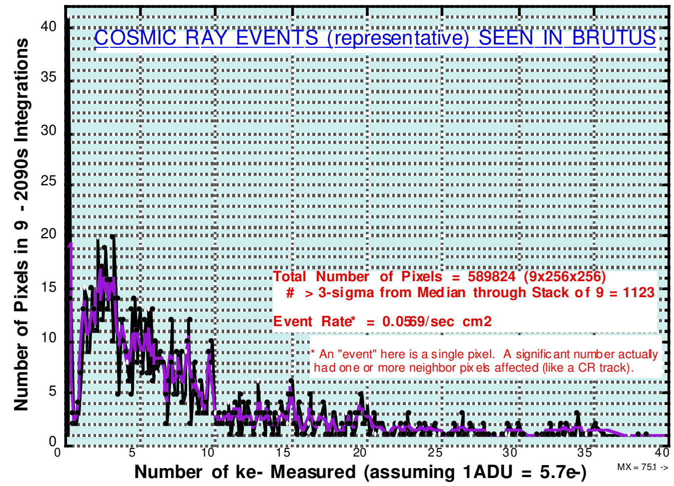

The ability of the NICMOS arrays to perform non-destructive readouts allows temporal sampling of the charge accumulation rate during integration. From this CR events can (for the most part) be identified, rejected, and corrected.

The NICMOS FPAs have very low pixel adjacency effects (cross-talk, charge migration, etc.) from proton-hit neighboring pixels. This was originally determined from data taken during a series of radiation exposure tests at the Harvard cyclotron where the proton beam geometry and energies were controllable. The accompanying figure illustrates the increment in measured charge in nine rows of pixels along two columns on either side of a column along which proton hits had occurred. This is from a statistical aggregate of 12 proton tracks which were oriented orthogonally with respect to the array read out direction. The mean count rates along the stacked proton tracks is 5270 ADU. As is evident, immediately adjacent neighboring pixels experience levels of charge elevation of only ~ 1/4%.

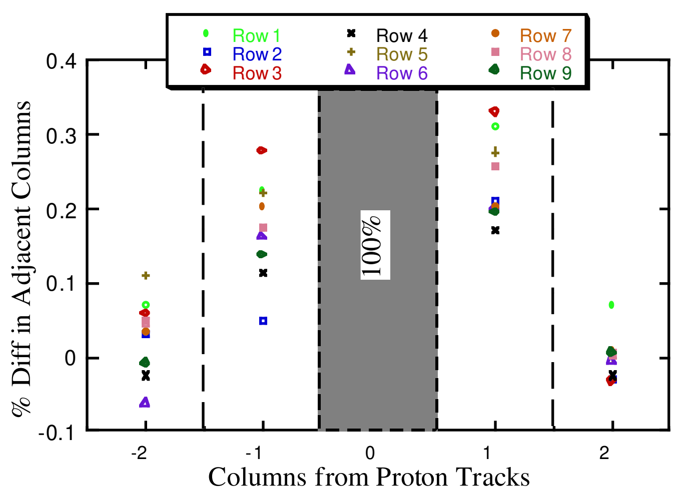

IMAGE QUALITY

The image quality of all three NICMOS cameras was ascertained in the RAS/HOMS facility at BATC following Centrifuge and acoustic stress testing at GSFC. A primary metric used for image quality is the total energy encircled to a given radius from the center of a PSF of a point image. The NICMOS optical system was designed to a set of encircled energy requirements specified for 1 micron light. The RAS/HOMS source delivery system produces an input beam at 0.81 microns, resulting in a spatially smaller PSF. Therefore, encircled energy measures have been made at both a 95mas radius (as per the CEI specification) and 77mas. The latter is appropriate to the rescaled image size of the PSF at 0.81 microns, specifically for Camera 1 which is critically sampled.. For cameras 2 and 3, as the pixelization and aberration contributions increase relative to the diffraction contribution, the larger radius measure is the more appropriate one to use for comparison of performance to specification. Encircled energies will be remeasured in orbit during SMOV. Although the image quality requirement is specified only for field center, measures have been made for this location and for the centers of each of the detector quadrants.

IMAGE QUALITY VIA ENCIRCLED ENERGY

Camera, Location	Pixel Size	95 mas Requir'mt	95 mas Measure	77 mas Measure
1, Center	43 mas	56 %	57.6 %[1]	53.3 %[2]
1, Quad 1			62.3 %	57.6 %
1, Quad 2			63.3 %	57.3 %
1, Quad 3			64.9 %	60.1 %
1, Quad 4			61.6 %	56.8 %
1, Average			61.9 %	57.0 %
2, Center	75 mas	42 %	70.6 %	62.6 %
2, Quad 1			53.3 %	44.9 %
2, Quad 2			65.0 %	58.8 %
2, Quad 3			63.3 %	54.5 %
2, Quad 4			60.1 %	51.1 %
2, Average			62.5 %	54.4 %
3, Center	199 mas	38 %	66.4 %	56.1 %
3, Quad 1			68.9 %	58.6 %
3, Quad 2			54.1 %	44.8 %
3, Quad 3			---- *	---- *
3, Quad 4			59.8 %	51.8 %
3, Average			62.3 %	52.8 %

1) C1, Center data taken at non-optimal PAM setting. Quads were optimized.
2) C3, Quad 3 background data was corrupted. Values suspect and not used.

EXTENDED PSF VERIFICATION

The performance of the NICMOS (Camera 2) coronagraph, in terms of both diffracted energy suppression from an occulted source and instrumental scattering, will be quantitatively assessed from on-orbit testing during SMOV. In an effort to gain some insight into this during ground testing, a series of both normally exposed and deeply overexposed images were taken in a series of spatial patterns in and out the coronagraphic hole. Because of system limitations in ground testing this could only be done at 0.81µm using the F110W filter.

A severely over exposed image, ~100,000 times full well depth in the central pixel of an unocculted PSF, is shown below. The spatial extent of the 256x256 pixel image is 19.2"-square on the sky. The inset image (6.75" on a side) was over-exposed to ~1000 times full well. The two together show the inner and outer portions of the extended PSF with a dynamic range of several million. In both images the central ~3-4 pixel radius region (roughly the size of the coronagraphic occulting spot) is saturated. The PSF matches very well to expectations based upon optical models of the NICMOS+HST (RAS/HOMS) system.

The circular feature centered on (X,Y) of ~(24,103) is apparently an image "ghost" from the extremely over-exposed target. For a well-exposed target the brightest features in the ghost would be approximately 100 times less than the read noise, and hence are normally both invisible and inconsequential.

Camera 2 - Extended PSF (Diffraction + Scattering)
0.81 micron Point Source, 100000x Full Well Exposure

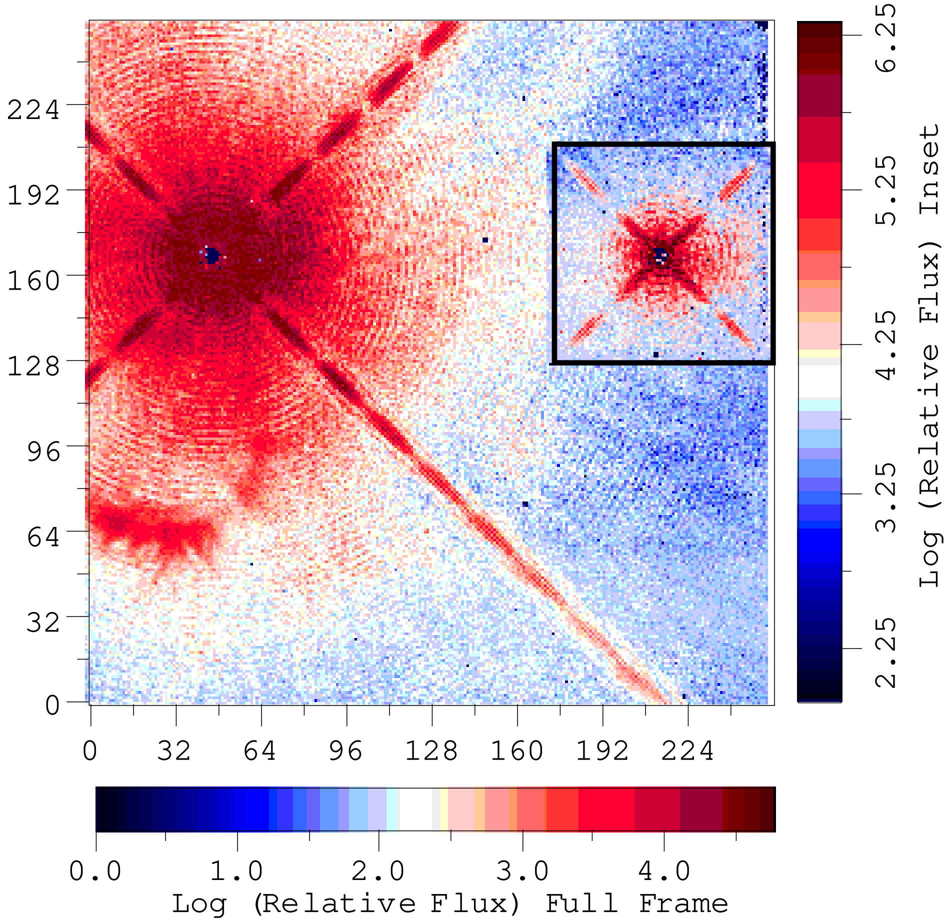

Software for generating model PSFs for the NICMOS+HST optical system was provided to the NICMOS IDT by R. Hook (ESA/HST-ECF).

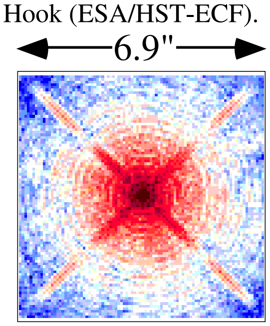

The S/W incorporates design specifications for the NICMOS optics and inputs from a CODE-V optical model of the instrument. Using this, a simulated PSF was generated for Camera 2 and a source wavelength of 0.81 mm (that of the laser in the RAS/HOMS system). The spatial extent of the simulation is just slightly larger then the inset observed PSF to the left. The fidelity of the simulation is readily apparent.

POLARIMETRIC CALIBRATION

NICMOS cameras 1 and 2 each contain a set of 3 polarizing elements made from Polarcore on a filter substrate to obtain bandpass isolation. The short wavelength polarizers, in Camera 1 transmit light in the spectral range 0.81 to 1.29 µm. The transmissivity of the Camera 2 polarizers is between 1.9 and 2.1 µm. The absolute orientation and efficiency of the NICMOS polarizers as well as the intrinsic instrumental polarization, and sensitivity of the camera 3 grisms to polarized light were measured using the CIRCE. stimulus. CIRCE provided a controllable source of polarized light. Background corrected intensity measures were obtained for each spectral element at 5° incremental steps of the CIRCE external polarizer over a range of 200° of rotation.

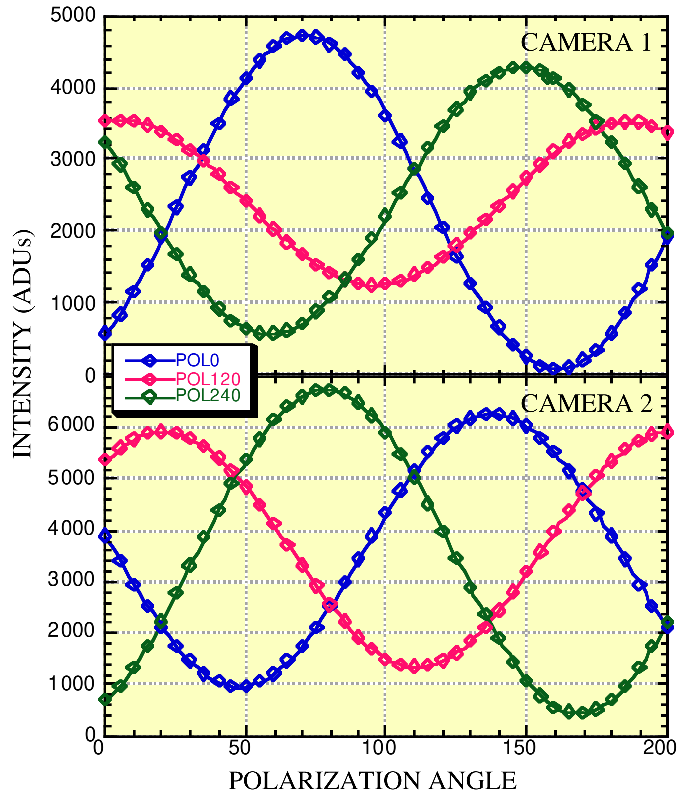

Intensity variations due to the polarizers were fit to a function of the usual form:

$$I = A + B \cos^2(\theta - \phi)$$

where: ϕ is the angle between the CIRCE rotation angle (θ) and the axis of the NICMOS polaroid. A and B are the intensity minimum and amplitude, respectively.

The efficiency of the polarizers defined by f = 100[p(measured)/p(incident)]%, assuming 100% polarized incident light, is simply f = 100[B/(2A + B)] and was found to be as follows:

EFFICIENCY OF THE NICMOS POLARIZERS (Percentage)

Camera	f(POL0)%	f(POL120)%	f(POL240)%
1	97.17±0.35	47.71±1.27	76.82±0.83
2	73.13±0.40	62.88±0.91	87.38±0.57

As measured from the NICMOS Aperture Offset Angle of 225°, about the aperture center toward the +U3 axis (see figure in Instrument Overview section), the polarizer orientation angles are:

POLARIZER ORIENTATIONS (relative NICMOS Aperture Offset Angle)

Cam	POL0	POL120	POL240	POL120 −POL0	POL240 −POL120	POL240 −POL0
1	1.42°±0.02°	116.30°±0.04°	258.72°±0.02°	114.88°	142.42°	257.30°
2	8.84°±0.05°	131.42°±0.03°	248.18°±0.04°	122.58°	116.76°	239.34°

SUMMARY OF RESULTS

1. NICMOS does analyze polarized light in a repeatable fashion.
2. Intrinsic instrumental polarization (measured through broadband filters) is very low, <~1%.
3. Efficiencies of polarizers are not identical, and lower than expected in the POL120 elements.
4. Orientation angles (and relative offsets) of polarizers are outside of the design goal envelope.
5. Camera 3 grisms are slightly sensitive to polarized light (≤ 1.5% intensity variations).

THE DEWAR "ANOMALY" AND CRYOGEN MANAGEMENT/LOSS

The integrated NICMOS FPAs will be maintained and operated, on-orbit, at 58K. The detectors are housed in a cold-well inside of a large dewar filled with solid N_2 suspended in a 1.6% fill-factor aluminum foam. The dewar, while in a vertical configuration, was filled with ~238 lbs. of liquid N_2 in December, 1995. The N_2 was then frozen by flowing liquid Helium at ~30K through a cooling coil located at the aft end of the dewar. The bulk temperature of the N_2 cooled to ~40K during this operation, but local areas in close thermal contact with the cooling coils were cooled further. On orbit, the parasitic heat leak into the dewar is ~130 milliWatts per day. This heat source results in a slow sublimation of solid N_2 which is vented to space through a capillary tube. At launch the dewar will have ~224 lbs. of cryogen as some was expended during thermal vacuum testing and also during early pre-flight cryogen management activities. We expect the cryogen to be depleted approximately 4.2 years after launch, which is the nominal NICMOS mission lifetime.

Normally, on the ground, the vent line valve is sealed (and will be opened by the flight crew on-orbit during NICMOS installation into HST). In ambient conditions the parasitic heat load is ~700 milliWatts/day, giving rise to an increase in the bulk temperature of the N_2 of ~0.3K per day. To keep the N_2 from reaching it's triple-point at ~63K, and boiling in the dewar, recooling operations are required. The N_2 is never allowed to rise beyond ~59K and is recooled before this. Just prior to shipping NICMOS to GSFC for acoustic/vibration testing in the spring of 1996, final adjustments were made to the optics in the FOB. This was done shortly after a recool where the bulk N_2 temperate was ~42K. On return to BATC it was discovered, while moving the PAM during routine focus check operations, that Camera 3 was "out of focus" with respect to Cameras 1 and 2. At that time the N_2 had warmed to ~56K and was scheduled for a recool. Subsequent investigation revealed that the high-elasticity aluminum tank had "stretched" by an overall length of ~6mm (relative to it's length at 42K where ther optical foci had been set). This was due to both the high elasticity of the aluminum tank, and the fact that the CTE of solid N_2 at these temperatures exceeds aluminumby ~25 times. It was found that the expansion and contraction of the N_2 during heating and cooling cycles causes the dewar tank to grow and shrink. This was looked at extensively from safety, structures, and materials standpoints and was found not to be a problem.

The detectors, however, are mechanically coupled to the front of the dewar, and hence are pushed out of their nominal focal positions. Both the different focal ratios of the three cameras, and the physically different location of the Camera 3 detector (further "back" in the cold well) result in contemporaneous non-parfocality at nominal operating temperatures. Because of the long focal ratios of Cameras 1 and 2, and the close physical proximity of thier detectors, these optical channels remain confocal. We expect that during the normal course of the mission, as cryogen sublimes and is vented, that the dewar shell will relax and the cold-well will return to it's nominal position at the equilibration temperature of the N_2 ice. We anticipate that this is unlikely to happen until at least 6 months into the mission, and perhaps may be as long as a year and a half.

It is important to note that there is more than sufficient range in the PAM to achieve in excellent in-focus images for all three cameras, but not simultaneously at this time. The PAM will be routinely used on-orbit to accommodate the need to refocus between Cameras 1/2 and Camera 3. Observers should recognize this in planning multi-camera cotemporaneous observations.

ACKNOWLEDGEMENTS

The authors and other members of the NICMOS science team gratefully acknowledge the diligent work, responsiveness, and attention to detail provided by the technical staff at BATC in the construction and testing of NICMOS. As a direct result, though there are some open minor performance issues, the as-built instrument meets it's high-level design requirements and is unequivocally ready flight. We would also like to acknowledge the many hours of tedious work done by many of the NICMOS postdoctoral associates in reducing and analyzing the SLTV data. Finally, we would like to specifically thank Michael Corbin and Dean Hines (UofA) for their contributions to the grism and polarimetric analyses summarized in this report.